Supporting Information for:

Nonlocal Response of Metallic Nanospheres Probed by Light, Electrons, and Atoms

Thomas Christensen,[†,‡] Wei Yan,[†,‡] Søren Raza,[†,¶] Antti-Pekka Jauho,[§,‡]

N. Asger Mortensen,[†,‡] and Martijn Wubs[*,†,‡]

DTU Fotonik, Center for Nanostructured Graphene, Center for Electron Nanoscopy, and DTU Nanotech

E-mail: mwubs@fotonik.dtu.dk

[*]To whom correspondence should be addressed

[†]Department of Photonics Engineering, Technical University of Denmark, DK-2800 Kgs. Lyngby, Denmark

[‡]Center for Nanostructured Graphene, Technical University of Denmark, DK-2800 Kgs. Lyngby, Denmark

[¶]Center for Electron Nanoscopy, Technical University of Denmark, DK-2800 Kgs. Lyngby, Denmark

[§]Department of Micro- and Nanotechnology, Technical University of Denmark, DK-2800 Kgs. Lyngby, Denmark

Hydrodynamic nonlocal interaction range ξ_{NL}

Table S1 provides a listing of typical values for the nonlocal interaction range $\xi_{\mathrm{NL}} = v_{\mathrm{F}}/\omega$ considered in the optical domain at a wavelength of 500 nm, computed from tabulated plasma frequencies for various relevant plasmonic metals.

Table S1: Table of values for the plasma frequency, ω_{p}, Fermi velocity, v_{F}, and nonlocal interaction range, ξ_{NL} (at a wavelength of 500 nm), for a selection of plasmonic metals.

Metal	$\hbar\omega_{\mathrm{p}}$ [eV]	v_{F} [10^6 m/s]	ξ_{NL} [Å]	Reference
Li	8.05	1.29	3.4	S1
Na	6.04	1.07	2.8	S1
Al	14.94	1.95	5.2	S2
K	4.39	0.86	2.3	S1
Cu	10.83	1.58	4.2	S3
Pd	9.72	1.47	3.9	S3
Ag	9.01	1.39	3.7	S3
Pt	9.59	1.45	3.9	S3
Au	9.03	1.40	3.7	S3

Measurement coefficients

In this section, we review the particulars of the Mie–Lorenz coefficient expansion of the extinction cross-section, σ_{ext}, the EELS probability, Γ, and the free-space normalized local density of states (LDOS), $\rho^{\mathrm{E}}/\rho_0^{\mathrm{E}}$. First, we briefly remind how a given exciting field can be decomposed into multipoles.

Multipole expansion of exciting field. With the relationship between exciting and scattered fields established, Eq. (3), the problem of deducing the scattered field due to some exciting field is reduced to expanding the exciting field in the multipole basis. As a consequence of the orthogonality of the vector wave functions on the surface of a sphere, the expansion coefficients can principally be obtained from:[S4]

$$a_{lm}^{\mathrm{ex}} = \frac{\int_0^{2\pi}\int_0^{\pi} \mathbf{E}^{\mathrm{ex}} \cdot \overline{\mathbf{M}}_{lm}^{[1]} \sin\theta \,\mathrm{d}\theta\mathrm{d}\phi}{\int_0^{2\pi}\int_0^{\pi} |\mathbf{M}_{lm}^{[1]}|^2 \sin\theta \,\mathrm{d}\theta\mathrm{d}\phi}, \tag{S1}$$

with $\overline{\mathbf{F}}$ denoting the complex conjugate of $\mathbf{F}$. An identical equation for b_{lm}^{ex} exists with $\mathbf{M}_{lm}^{[1]}$ replaced by $\mathbf{N}_{lm}^{[1]}$.

At this point, it is worthwhile noting that the inclusion of hydrodynamics incurs no additional analytical difficulties in the external region, compared to local theory; all results from local theory remain valid for $r > R$, provided the local TM Mie–Lorenz coefficients are supplemented by the hydrodynamic correction Δ_l from Eq. (4c). As such, for measurements restricted to the external region, hydrodynamics can be immediately included using well-established results from local theory. In the internal region, the additional wave components due to the longitudinal multipoles, $\mathbf{L}_{lm}^{[1]}$, break this convenient correspondence. In the following we consider evaluation of the extinction cross-section, the EELS probability and the electric LDOS in the external region.

Extinction cross-section. In the case of an incident plane wave, propagating along the z-direction and polarized along the x-direction, $\mathbf{E}^{\text{ex}}(\mathbf{r}) = \mathrm{e}^{ik_{\text{D}}z}\hat{\mathbf{e}}_x$, the exciting field can be decomposed in a multipole basis with $m = \pm 1$, leading to expansion coefficients:[S4]

$$a_{lm}^{\text{ex}} = E_l m \delta_{|m|1}\,, \qquad\qquad b_{lm}^{\text{ex}} = E_l \delta_{|m|1}, \tag{S2}$$

with $E_l = -i^{l+1}(2l+1)/[2l(l+1)]$.

The extinction cross-section, σ_{ext}, which measures the ratio of power dissipated due to both scattering and absorption by the sphere, W_{ext}, to the incident intensity, I_0, can be obtained by application of the optical theorem,[S5] giving;

$$\boxed{\sigma_{\text{ext}} = \frac{W_{\text{ext}}}{I_0} = \frac{2\pi}{k_{\text{D}}^2}\sum_{l=1}^{\infty}(2l+1)\mathrm{Re}\left(t_l^{\text{TE}} + t_l^{\text{TM}}\right).} \tag{S3}$$

For discussion of actual results, we prefer the dimensionless extinction efficiency $Q_{\text{ext}} = \sigma_{\text{ext}}/\pi R^2$ rather than the cross-section. Regardless of the choice of efficiency or cross-section, the characteristics of the extinction closely mirrors those of standard experimental transmission measurements on widely separated particle arrays.

Electron energy loss probability with aloof electron. The case of the EELS probability for aloof electron trajectories is also approachable by expansion in the multipole basis. In particular, an electron traveling at constant velocity $\mathbf{v} = v\hat{\mathbf{z}}$ with $t = 0$ impact parameter $\boldsymbol{b}$ in the xy-plane, emanates a cylinder-like wave from the electron trajectory $\mathbf{r}_{\text{e}}(t) = \boldsymbol{b} + \mathbf{v}t$. Specifically, if $\mathbf{b} = 0$ the traveling charge density is $\rho(\mathbf{r}, t) = -e\delta(\mathbf{r} - \mathbf{v}t)$ which excites an electric field $\mathbf{E}^{\text{ex}}(\mathbf{r}, \omega) = \frac{e\omega}{2\pi\varepsilon_0 v^2\gamma\varepsilon}\mathrm{e}^{i\omega z/v}\left[\frac{i}{\gamma}K_0\left(\frac{\omega r_\parallel}{v\gamma}\right)\hat{\mathbf{z}} - K_1\left(\frac{\omega r_\parallel}{v\gamma}\right)\hat{\mathbf{r}}_\parallel\right]$ with $\gamma = 1/\sqrt{1-(v/c)^2}$ denoting the Lorentz contraction factor.[S6,S7] This incident field scatters off the metallic sphere, and the scattered field,

working back on the electron, incurs a measurable energy loss, ΔE, for the total electron energy

$$\Delta E = e \int_{-\infty}^{\infty} \mathbf{E}^{\mathrm{sc}}[\mathbf{r}_{\mathrm{e}}(t), t] \cdot \mathbf{v}\, \mathrm{d}t. \tag{S4}$$

The loss can also be expressed in terms of a frequency-decomposition through $\Delta E \equiv \int_0^\infty \hbar\omega\Gamma(\omega)\, \mathrm{d}\omega$, with $\Gamma(\omega)$ denoting the electron loss probability. The time-domain scattered field in Eq. (S4) can be represented by its frequency-domain Fourier components, which, together with the definition of $\Gamma(\omega)$ and the property $\mathbf{E}(\mathbf{r}, \omega) = \overline{\mathbf{E}}(\mathbf{r}, -\omega)$, allows expression of $\Gamma(\omega)$ in terms of the scattered field:

$$\Gamma(\omega) = \frac{ev}{\pi\hbar\omega} \int_{-\infty}^{\infty} \hat{\mathbf{z}} \cdot \mathrm{Re}\left\{ \mathbf{E}^{\mathrm{sc}}[\mathbf{r}_{\mathrm{e}}(t), \omega] \mathrm{e}^{-i\omega t} \right\} \mathrm{d}t. \tag{S5}$$

The problem of determining the appropriate multipole expansion of the exciting field due to the traversing electron, and the subsequent integration of the induced field as required to obtain $\Gamma(\omega)$ through Eq. (S5), was solved by F. J. García de Abajo in Ref. S8 for the case of a sphere embedded in vacuum, $\varepsilon_{\mathrm{D}} = 1$, and for aloof electron trajectories, $|\boldsymbol{b}| = b > R$. The resulting expression is:[S7,S8]

$$\boxed{\Gamma(\omega) = \frac{\alpha}{\omega} \sum_{l=1}^{\infty} \sum_{m=-l}^{l} K_m^2\left(\frac{\omega b}{v\gamma}\right) \left[C_{lm}^{\mathrm{TE}} \mathrm{Re}(t_l^{\mathrm{TE}}) + C_{lm}^{\mathrm{TM}} \mathrm{Re}(t_l^{\mathrm{TM}}) \right],} \tag{S6}$$

where $\alpha = \frac{e^2}{\hbar c} \frac{\varepsilon_0}{4\pi}$ is the fine-structure constant, K_m denotes the modified Bessel function of the second kind of order m, and C_{lm}^{TE} and C_{lm}^{TM} are functions of l, m, and v/c given by:[S7]

$$C_{lm}^{\mathrm{TE}} = \frac{1}{l(l+1)} |2m\Pi_{lm}|^2, \qquad C_{lm}^{\mathrm{TM}} = \frac{1}{l(l+1)} \left| \frac{c}{v\gamma} \Xi_{lm} \right|^2, \tag{S7a}$$

with

$$\Pi_{lm} = \sqrt{\frac{(2l+1)}{\pi} \frac{(l-|m|)!}{(l+|m|)!}} \frac{(2|m|-1)!!}{(v\gamma/c)^{|m|}} C_{l-|m|}^{(|m|+1/2)}\left(\tfrac{c}{v}\right), \tag{S7b}$$

$$\Xi_{lm} = \Pi_{l,m+1} \sqrt{(l+m+1)(l-m)} + \Pi_{l,m-1} \sqrt{(l-m+1)(l+m)}, \tag{S7c}$$

where $C_n^{(\nu)}(x)$ denotes the nth Gegenbauer polynomial of order ν.[S9]

Lastly, we note that the relativistic kinetic energy of the electron, E_e, relates to its velocity, v, through $E_e = m_e\gamma c^2 - m_e c^2$, where m_e denotes the electron mass. Consequently, a given

kinetic electron energy E_e corresponds to the velocity

$$\frac{v}{c} = \sqrt{1 - \left(\frac{m_e c^2}{E_e + m_e c^2}\right)^2}. \tag{S8}$$

Local density of states. The third and final relevant excitation field and measurement to be considered here, is that of an electric dipole field and a measurement of the LDOS, relevant *e.g.*, for the spontaneous decay of an electric dipole emitter near the sphere. The problem of dipole radiation outside a sphere was first considered by M. Kerker *et al.* in Ref. S10 using the multipole basis, in the context of surface enhanced Raman scattering (SERS). Subsequently, the problem of decay rates of emitters near metallic and dielectric spheres was treated, relating the Mie–Lorenz coefficients to the decay rate enhancement.[S11,S12]

The partial electric LDOS experienced by an emitter of transition frequency ω with its dipole-moment oriented along the radial and tangential directions, $\rho^{\mathrm{E}}_{\perp}$ and $\rho^{\mathrm{E}}_{\parallel}$, respectively, at a distance $b > R$ from origo is given by:[S12,S13]

$$\boxed{\begin{aligned} \frac{\rho^{\mathrm{E}}_{\perp}}{\rho^{\mathrm{E}}_{0}} &= 1 + \frac{3}{2}\frac{1}{y^2}\sum_{l=1}^{\infty}(2l+1)l(l+1)\mathrm{Re}\left[t_l^{\mathrm{TM}} h_l^{(1)}(y)^2\right], \\ \frac{\rho^{\mathrm{E}}_{\parallel}}{\rho^{\mathrm{E}}_{0}} &= 1 + \frac{3}{4}\frac{1}{y^2}\sum_{l=1}^{\infty}(2l+1)\mathrm{Re}\left[t_l^{\mathrm{TE}}\xi_l(y)^2 + t_l^{\mathrm{TM}}\xi_l'(y)^2\right], \end{aligned}} \tag{S9}$$

where ρ^{E}_0 denotes the LDOS in the absence of the sphere $\rho^{\mathrm{E}}_0 = \omega^2/\pi^2 c^3$, $y = k_{\mathrm{D}} b$ denotes phase-accumulation from dipole to sphere, and finally ξ_l denotes the Riccati-Bessel function $\xi_l(y) = y h_l^{(1)}(y)$ introduced for brevity of notation. The orientation-averaged LDOS, ρ^{E}, can be obtained from the partial LDOS through summation[S14,S15] $\rho^{\mathrm{E}} = \frac{1}{3}\rho^{\mathrm{E}}_{\perp} + \frac{2}{3}\rho^{\mathrm{E}}_{\parallel}$.

We note that the radially oriented emitter couples solely with TM-polarized fields, while the tangentially oriented emitter couples to both TM and TE polarizations. However, for small spheres and probe distances, $y \ll 1$, the TM contribution dominates the TE contribution as can be verified from the $0 < x \ll \sqrt{l+1}$ asymptotic behavior of $\xi_l(x) \simeq N_{l+1}x^{l+1} - iN_l^{-1}x^{-l}$ and $\xi_l'(x) \simeq (l+1)N_{l+1}x^l + ilN_l^{-1}x^{-l-1}$ with $N_l = 2^l l!/(2l)!$. As a consequence, we expect strong enhancement of either radial or tangential LDOS to arise primarily due to TM polarized interaction.

Asymptotics of LDOS and EELS - similarities with extinction

It is instructive to consider the limits in which the LDOS and EELS spectra are qualitatively similar to the extinction spectra, in other words, to study the regimes wherein extinction measurements gives information directly comparative to EELS or LDOS measurements on the same system. In this section, we derive asymptotic expressions for the normalized orientation-averaged LDOS in the large-separation range, $k_D b \gg 1$, and similarly for the EELS signal in the ultra-relativistic limit, $v/c \to 1$. We show that these asymptotics display the same qualitative behavior as the full extinction spectra, apart from minor probe-related differences.

LDOS at large surface-to-probe separations. We consider the large-y limit of Eqs. (S9), corresponding to probe-to-surface separations exceeding the wavelength in the surrounding dielectric. From the large-argument asymptotics[S16] of the spherical Hankel and Ricatti-Bessel functions [$h_l^{(1)}(y) \simeq i^{-l-1}y^{-1}e^{iy}$, $\xi_l(y) \simeq i^{-l-1}e^{iy}$, and $\xi_l'(y) \simeq i^{-l}e^{iy}$ valid for $y \gg 1$] we find that Eq. (S9) reduces to:

$$\frac{\rho_\perp^E}{\rho_0^E} = 1 + \frac{3}{2}\frac{1}{y^4}\sum_{l=1}^{\infty}(2l+1)l(l+1)\mathrm{Re}\left[t_l^{TM}e^{2iy}\right](-1)^{l+1}, \tag{S10a}$$

$$\frac{\rho_\parallel^E}{\rho_0^E} = 1 + \frac{3}{4}\frac{1}{y^2}\sum_{l=1}^{\infty}(2l+1)\mathrm{Re}\left[(t_l^{TE} - t_l^{TM})e^{2iy}\right](-1)^{l+1}, \tag{S10b}$$

which, for the orientation-averaged normalized LDOS, to lowest order in y^{-2}, gives:

$$\frac{\rho^E}{\rho_0^E} = 1 + \frac{1}{2}\frac{1}{y^2}\sum_{l=1}^{\infty}(2l+1)\mathrm{Re}\left[(t_l^{TE} - t_l^{TM})e^{2iy}\right](-1)^{l+1}, \tag{S11}$$

valid for $y \gg 1$. Apart from scaling, the factor e^{2iy}, which is due to interference of emitted and reflected waves, and some signs, this form is qualitatively similar to the form of the extinction spectra in (S3). In particular, the same $(2l+1)$ magnitude of the weighting is present. This illustrates why just the dipolar term is significant in the large separation limit for small spheres, where t_1^{TM} is logarithmically dominant compared to the remaining Mie–Lorenz coefficients.

EELS signal in ultra-relativistic limit. In the $v/c \to 1$ limit we can evaluate the Gegenbauer polynomials at unity argument using[S17] $C_n^{(\nu)}(1) = (2\nu + n - 1)!/[(2\nu - 1)!n!]$ - this value is approached linearly or quadratically as a function of the argument, depending on the parity of n. The limit $v/c \to 1$ also sends $\gamma \to \infty$, but a sub-linear rate of divergence. As such, we evaluate

the limit $v/c \to 1$ in Eq. (S6), but retain γ as finite. To lowest order in γ^{-2} we find after some manipulations that $C_{lm}^{\text{TE,TM}} \simeq \pi^{-1}\gamma^{-2}(2l+1)\delta_{|m|,1}$, leading to:

$$\Gamma(\omega) = \frac{\alpha}{\omega}\frac{2}{\pi\gamma^2}K_1^2\left(\frac{\omega b}{v\gamma}\right)\sum_{l=1}^{\infty}(2l+1)\text{Re}\left[t_l^{\text{TE}} + t_l^{\text{TM}}\right], \tag{S12}$$

valid for v/c near unity, *i.e.*, for ultra-relativistic electron velocities. Evidently, apart from the two frequency-terms outside the sum, the spectral response is identical to that obtained for extinction in Eq. (S3), and as such provides an identical weighting to the various multipoles. Effectively, then, the dipole is the prominent peak due to the dominance of t_1^{TM} relative to the remaining Mie–Lorenz coefficients, at least for small spheres.

Finally, from the $x \gg m$ asymptotic form of the modified Bessel function,[S9] $K_m^2(x) \simeq \frac{\pi}{2x}\text{e}^{-2x}$, it is evident that the loss probability decays approximately exponentially in the far-probe region. Due to Lorenz contraction, the transition to the far-probe region is postponed until the contracted distance b/γ is comparable with the electron wavenumber ω/v.

Multipolar polarizability and nonretarded plasmon resonances

We can derive the nonretarded multipolar polarizability, α_l, giving the response to incident potentials of pole order $l+1$, from the Mie–Lorenz coefficients, by noting the interrelationship[S18]

$$\alpha_l = \lim_{c/\omega R\to\infty}\left[-\frac{4\pi i\mathcal{N}_l}{k_{\text{D}}^{2l+1}}t_l^{\text{TM}}\right], \tag{S13}$$

with $\mathcal{N}_l = \frac{l[(2l+1)!!]^2}{(l+1)(2l+1)}$. This allows determination of the hydrodynamic multipolar polarizability, using Eqs. (4), and yields [upon using the small-argument limiting forms of the spherical Bessel and Hankel functions, namely $j_l(x) \simeq x^l/(2l+1)!!$ and $h_l^{(1)}(x) \simeq x^l/(2l+1)!! - i(2l-1)!!/x^{l+1}$ valid for $x \ll \sqrt{l+1}$]:

$$\alpha_l = 4\pi R^{2l+1}\frac{l\left[\varepsilon_{\text{M}} - \left(1+\delta_l\right)\varepsilon_{\text{D}}\right]}{l\varepsilon_{\text{M}} + (l+1)\left(1+\delta_l\right)\varepsilon_{\text{D}}}, \tag{S14}$$

with $\delta_l = \Delta_l/[j_l(x_{\text{M}})(l+1)]$, see Eq. (4c). The hydrodynamic correction δ_l vanishes in the local limit, such that α_l appropriately reduces to the local response approximation (LRA) multipolar polarizability $\alpha_l^{\text{L}} = 4\pi R^{2l+1}\frac{l(\varepsilon_{\text{M}}-\varepsilon_{\text{D}})}{l\varepsilon_{\text{M}}+(l+1)\varepsilon_{\text{D}}}$. The hydrodynamic multipolar polarizability was also considered by Fuchs and Claro in Ref. S19, through their more general consideration of the multipolar polarizability of a sphere with dielectric constant $\varepsilon(k,\omega)$. The form of Eq. (S14), however, is more elucidating in the direct comparison of hydrodynamic and local models.

Notably, the above form reinforces an idea of hydrodynamics as acting to effectively modify the neighboring dielectric surrounding,[S20] rendering it weakly frequency- and l-dependent.

The nonretarded plasmon condition, Eq. (6), is obtained immediately from the poles of the polarizability.

Mie–Lorenz transmission coefficients

In analogy with the *scattering* coefficients $t_l^{\mathrm{TE,TM}}$ discussed in Eq. (3), it is natural to introduce *transmission* coefficients $q_l^{\mathrm{TE,TM,L}}$ for the multipoles transmitted into the interior of the sphere:

$$a^{\mathrm{tr}}_{lm} = q^{\mathrm{TE}}_{l'} a^{\mathrm{ex}}_{l'm'} \delta_{ll'} \delta_{mm'}, \qquad b^{\mathrm{tr}}_{lm} = q^{\mathrm{TM}}_{l'} b^{\mathrm{ex}}_{l'm'} \delta_{ll'} \delta_{mm'}, \qquad c^{\mathrm{tr}}_{lm} = q^{\mathrm{L}}_{l'} b^{\mathrm{ex}}_{l'm'} \delta_{ll'} \delta_{mm'}. \tag{S15}$$

Note that the longitudinal multipoles, $\mathbf{L}^{\mathrm{tr}}_{lm}$, are excitable only by the ingoing TM multipoles, $\mathbf{N}^{\mathrm{ex}}_{lm}$, but not by ingoing TE multipoles, $\mathbf{M}^{\mathrm{ex}}_{lm}$ – a fact that is directly tied with the invariance of the TE scattering coefficients, t_l^{TE}, under inclusion of longitudinal waves.

Matching of the fields and currents at the boundary of the sphere yields expressions for the transmission coefficients, here given in terms of the scattering coefficients from Eqs. (4):

$$q_l^{\mathrm{TE}} = \frac{t_l^{\mathrm{TE}} h_l^{(1)}(x_{\mathrm{D}}) + j_l(x_{\mathrm{D}})}{j_l(x_{\mathrm{M}})}, \tag{S16a}$$

$$q_l^{\mathrm{TM}} = \frac{t_l^{\mathrm{TM}} h_l^{(1)}(x_{\mathrm{D}}) + j_l(x_{\mathrm{D}})}{j_l(x_{\mathrm{M}})} \sqrt{\frac{\varepsilon_{\mathrm{D}}}{\varepsilon_{\mathrm{M}}}}, \tag{S16b}$$

$$q_l^{\mathrm{L}} = l(l+1) \frac{t_l^{\mathrm{TM}} h_l^{(1)}(x_{\mathrm{D}}) + j_l(x_{\mathrm{D}})}{j_l'(x_{\mathrm{NL}})} \left(\frac{\varepsilon_{\mathrm{D}}}{\varepsilon_\infty} - \frac{\varepsilon_{\mathrm{D}}}{\varepsilon_{\mathrm{M}}} \right). \tag{S16c}$$

Longitudinal modes and approximate bulk plasmons

In this section, we consider an approximate criterion for the existence of bulk plasmons in finite or semi-finite metallic structures, and in particular derive Eq. (9).

In analogy with Eqs. (10), the governing equations, Eqs. (1), can be recast solely in terms of the current density (omitting explicit declaration of frequency dependence):

$$\left(\nabla^2 + k_{\mathrm{M}}^2\right) \nabla \times \mathbf{J}(\mathbf{r}) = 0, \tag{S17a}$$

$$\left(\nabla^2 + k_{\mathrm{NL}}^2\right) \nabla \cdot \mathbf{J}(\mathbf{r}) = 0, \tag{S17b}$$

By performing a spatial Fourier transform, and thus letting $\nabla \to i\mathbf{q}$, it is clear that Eq. (S17a)

describes the transverse (divergence-free or solenoidal) part of the current, while Eq. (S17b) describes the longitudinal (curl-free or irrotational) part of the current. In extended, infinite structures it is well-known that plasmon resonances above the plasma-frequency are inherently longitudinal. By extension, we introduce the assumption that bulk plasmons in finite structures are also solely longitudinal – thus effectively neglecting interaction with transverse light, thereby constituting the approximation in our following considerations.

To find longitudinal current density solutions, we examine the existence of solutions to Eqs. (S17) which are curl-free (*i.e.*, $\nabla \times \mathbf{J} = 0$). This condition can be satisfied by expressing the current density *via* a scalar velocity potential $\psi(\mathbf{r})$ through $\mathbf{J}(\mathbf{r}) \equiv \nabla\psi(\mathbf{r})$, since the curl of a gradient is always zero. With these assumptions for $\mathbf{J}(\mathbf{r})$ Eq. (S17a) is automatically fulfilled, and Eq. (S17b) reduces to a scalar equation for $\psi(\mathbf{r})$:

$$\left(\nabla^2 + k_{\mathrm{NL}}^2\right) \nabla^2\psi(\mathbf{r}) = 0. \tag{S18}$$

The potential $\psi(\mathbf{r})$ may be expanded in any complete, orthogonal set of functions, say $\{\psi_\nu(\mathbf{r})\}_{\nu=1}^{\infty}$, such that

$$\psi(\mathbf{r}) = \sum_\nu d_\nu \psi_\nu(\mathbf{r}), \tag{S19}$$

For the solution of Eqs. (S17) in a bounded domain Ω we only need to impose the additional BC that the normal component of the current density vanishes at the boundary $\partial\Omega$, *i.e.*, that $\hat{\mathbf{n}} \cdot \mathbf{J}(\mathbf{r}) = 0$ for $\mathbf{r} \in \partial\Omega$ with $\hat{\mathbf{n}}$ denoting the normal unit vector to $\partial\Omega$. By requiring that each component of the set $\{\psi_\nu(\mathbf{r})\}_{\nu=1}^{\infty}$ respects this BC, we impose the homogeneous Neumann BC that $\hat{\mathbf{n}} \cdot \nabla\psi_\nu(\mathbf{r})$ vanishes on the boundary $\partial\Omega$. A particularly convenient choice for the generating potentials can be constructed from the solutions of the Helmholtz equation,

$$\left(\nabla^2 + \kappa_\nu^2\right) \psi_\nu(\mathbf{r}) = 0, \tag{S20}$$

which constitute a complete, orthogonal set.

Applying the expansion in Eq. (S19), along with property of Eq. (S20), to Eq. (S18) determines the allowed values of the nonlocal propagation constants as $k_{\mathrm{NL}}^2 = \kappa_\nu^2$. Using the definition for k_{NL}^2 we finally obtain the longitudinal resonance frequencies in terms of the eigenvalues, κ_ν^2, of the Neumann BC Helmholtz equation

$$\omega_\nu(\omega_\nu + i\eta) = \frac{\omega_{\mathrm{p}}^2}{\varepsilon_\infty(\omega_\nu)} + \kappa_\nu^2\beta_{\mathrm{F}}^2, \tag{S21}$$

which describes the dispersion of hydrodynamic longitudinal modes in an arbitrary geometry.

The problem of determining the dispersion or resonance frequencies of bulk plasmons in any metallic structure is thus simplified to finding the eigenvalues of the Neumann BC Helmholtz equation. A similar result was obtained in Ref. S21 for the case of a metallic sphere.

By rescaling the Helmholtz equation through $\mathbf{x} = \mathbf{r}/R$, where R denotes some geometrically characteristic distance (such as the radius in a spherical geometry), the size-dependence of the resonances can be discerned. Specifically, by this rescaling, the eigenvalues of the dimensionless Helmholtz equation $(\nabla^2_{\mathbf{x}} + w_\nu^2)\psi(\mathbf{x})$ occur at $w_\nu = \kappa_\nu R$. Consequently, the resonance condition, Eq. (S21), can be cast in terms of the dimensionless eigenvalues w_ν:

$$\omega_\nu(\omega_\nu + i\eta) = \frac{\omega_\mathrm{p}^2}{\varepsilon_\infty(\omega_\nu)} + \frac{w_\nu^2\beta_\mathrm{F}^2}{R^2}, \tag{S22}$$

highlighting the size-dependent R^2-scaling of the bulk plasmons.

For a spherical geometry, the bounded solutions of the Helmholtz equation are $\psi_{lm}(x, \theta, \phi) = j_l(w_\nu x)P_l^m(\cos\theta)\mathrm{e}^{im\phi}$ as discussed also in the Methods section. Upon application of the Neumann BC at $x = 1$ (corresponding to $r = R$), the eigenvalues are seen to be solutions of the transcendental equation $j_l'(w_n) = 0$.

Quasistatic LDOS and $R = 10$ nm Drude-metal sphere

In this section we provide supporting calculations for the discussions related to Figure 8 of the main text, for a larger sphere of $R = 10$ nm. For a larger sphere inclusion of additional multipoles are required, compared to the 50 multipoles included for $R = 2.5$ nm, to achieve computational convergence (since the multipole resonances are positioned more densely). For computational purposes, it is convenient to work in the electrostatic regime for $l_\mathrm{max} > 50$ to avoid numerical instability associated with evaluation of high-order spherical Bessel functions. In this section, we therefore briefly discuss how to derive the electrostatic limit of the electric LDOS enhancement - an approximation which remains representative of the essential physics for an $R = 10$ nm sphere, provided b/R is not too large.

The electrostatic form for the LDOS enhancement can be recovered by considering the $c/\omega R \sim \lambda/R \to \infty$ asymptotics of the retarded expressions in Eqs. (S9). For this purpose we note the small-argument asymptotic forms $h_l^{(1)}(y) \simeq -i(2l-1)!!y^{-l-1}$ and $\xi_l'(y) \simeq il(2l-1)!!y^{-l-1}$, the connection between the TM Mie–Lorenz coefficients and the multipole polarizability in

Eq. (S13), and finally that the contribution from TE components vanish in the considered limit:[S22]

$$\frac{\rho^{\mathrm{E}}_{\perp}}{\rho^{\mathrm{E}}_{0}} = 1 + \frac{3}{2}\frac{1}{k_{\mathrm{D}}^{3}}\sum_{l=1}^{\infty}(l+1)^{2}\frac{1}{b^{2(l+2)}}\mathrm{Im}\left(\frac{\alpha_{l}}{4\pi}\right), \tag{S23a}$$

$$\frac{\rho^{\mathrm{E}}_{\parallel}}{\rho^{\mathrm{E}}_{0}} = 1 + \frac{3}{4}\frac{1}{k_{\mathrm{D}}^{3}}\sum_{l=1}^{\infty}l(l+1)\frac{1}{b^{2(l+2)}}\mathrm{Im}\left(\frac{\alpha_{l}}{4\pi}\right), \tag{S23b}$$

which, for the orientation-averaged LDOS, $\rho^{\mathrm{E}} = \frac{1}{3}\rho^{\mathrm{E}}_{\perp} + \frac{2}{3}\rho^{\mathrm{E}}_{\parallel}$, yields:

$$\frac{\rho^{\mathrm{E}}}{\rho^{\mathrm{E}}_{0}} = 1 + \frac{1}{2}\frac{1}{k_{\mathrm{D}}^{3}}\sum_{l=1}^{\infty}(2l+1)(l+1)\frac{1}{b^{2(l+2)}}\mathrm{Im}\left(\frac{\alpha_{l}}{4\pi}\right). \tag{S23c}$$

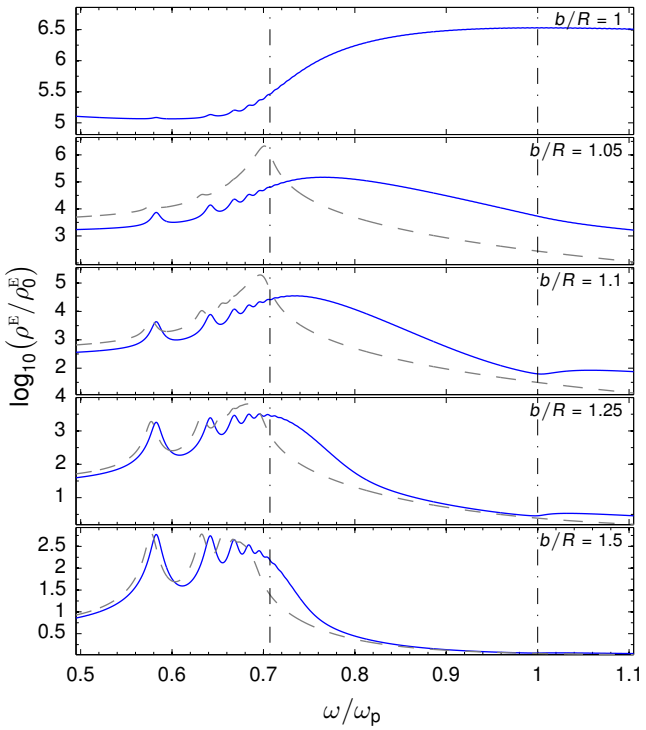

Figure S1: Logarithm of the normalized LDOS in hydrodynamic and LRA treatments, in full blue and dashed gray, respectively, for a $R = 10\,\mathrm{nm}$ sphere with Drude-metal composition ($\omega_{\mathrm{p}} = 10\,\mathrm{eV}$, $\eta = 0.1\,\mathrm{eV}$, and $\varepsilon_{\infty} = \varepsilon_{\mathrm{D}} = 1$). Calculated in the electrostatic approximation *via* Eq. (S23c) with 250 multipoles, *i.e.*, with $l_{\mathrm{max}} = 250$.

In Figure S1 we depict the results of an electrostatic calculation of the LDOS for an $R = 10\,\mathrm{nm}$ Drude-metal sphere. The electrostatic calculation gives representative results in the considered parameter-space, apart from a missing redshift ($\sim 19\,\mathrm{meV}$ for the dipole resonance) due to radiation reaction for both LRA and hydrodynamic treatments. Interestingly, the results show

that hydrodynamics predicts distinct differences from the LRA not only for small spheres, but also for larger spheres, provided the probe-to-surface separation, $b - R$, is sufficiently small. The disparity arises due to the lifting of the singular pile-up of modes predicted by the LRA near the planar-interface resonance at $\omega_p/\sqrt{2}$. As the probe approaches the surface additional multipoles are excited, until, *at* the surface, all multipoles in the spectral vicinity contribute. This suggests an alternate approach for examining the presence of nonlocal effects, even in large structures: consider the LDOS enhancement spectrally for short probe-to-surface distances. Both a significant broadening and a spectral shift of the peak LDOS enhancement is predicted by hydrodynamics compared to the LRA.

Finally, for intermediate separations, $b/R = 1.1$ and $b/R = 1.25$, the existence of low-order bulk plasmons produce a shoulder above ω_p – for shorter probe-to-surface separations the excitation of high-order multipole LSPs, existing above ω_p, overshadow this effect.

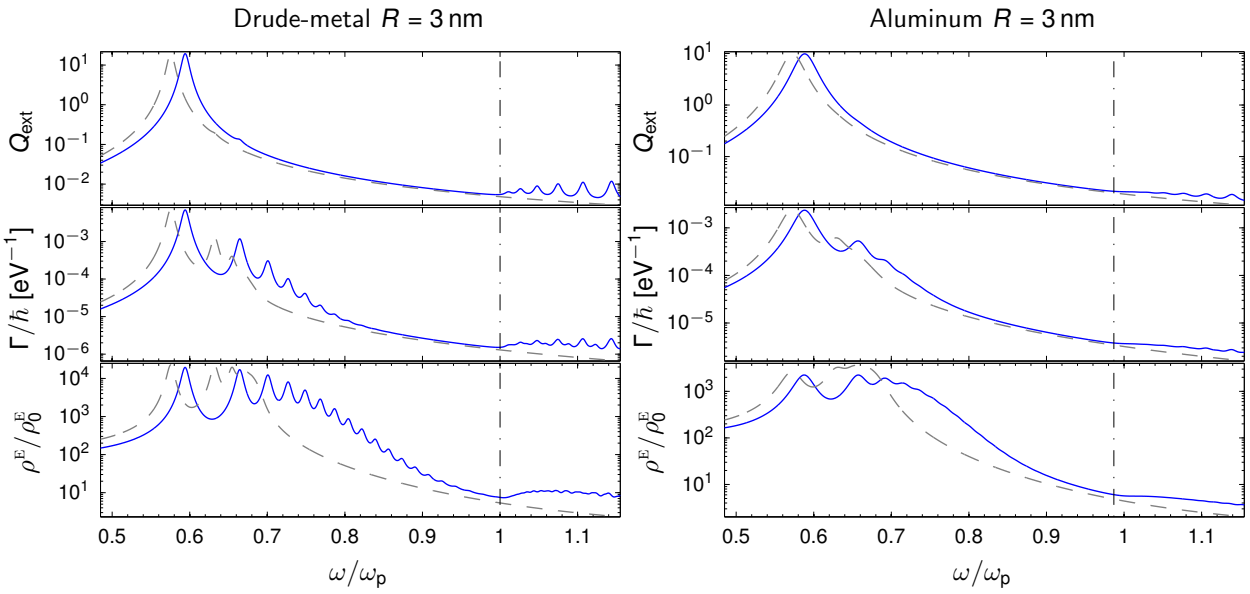

Figure S2: Extinction efficiency, EELS probability, and normalized LDOS. Setup parameters are identical to those in Figure 7, but with radius $R = 3$ nm and $b/R = 1.5$ (corresponding to maintaining the same probe-to-surface separation, 1.5 nm, as in Figure 7). Hydrodynamics and LRA in full blue and dashed gray, respectively, as before. Screened plasma frequency in dash-dotted black.

Additional spectra for larger nanospheres and for silver

To support the discussion related to Figure 7 of the main text, we here give additional calculations for a Drude-metal and aluminum in nanospheres with $R = 3$ nm in Figure S2. Clearly, to observe

the multipole features discussed in the main text the particles under consideration should be rather small – however, even at $R = 3\,\mathrm{nm}$ at least 3 multipole resonances are discernible for aluminum.

Lastly, we give calculations for silver in $R = 1.5\,\mathrm{nm}$ and $R = 3\,\mathrm{nm}$ nanospheres in Figure S3. For the case of silver the effects of higher-order multipoles are entirely suppressed by the strongly dispersive background due to the bound response.

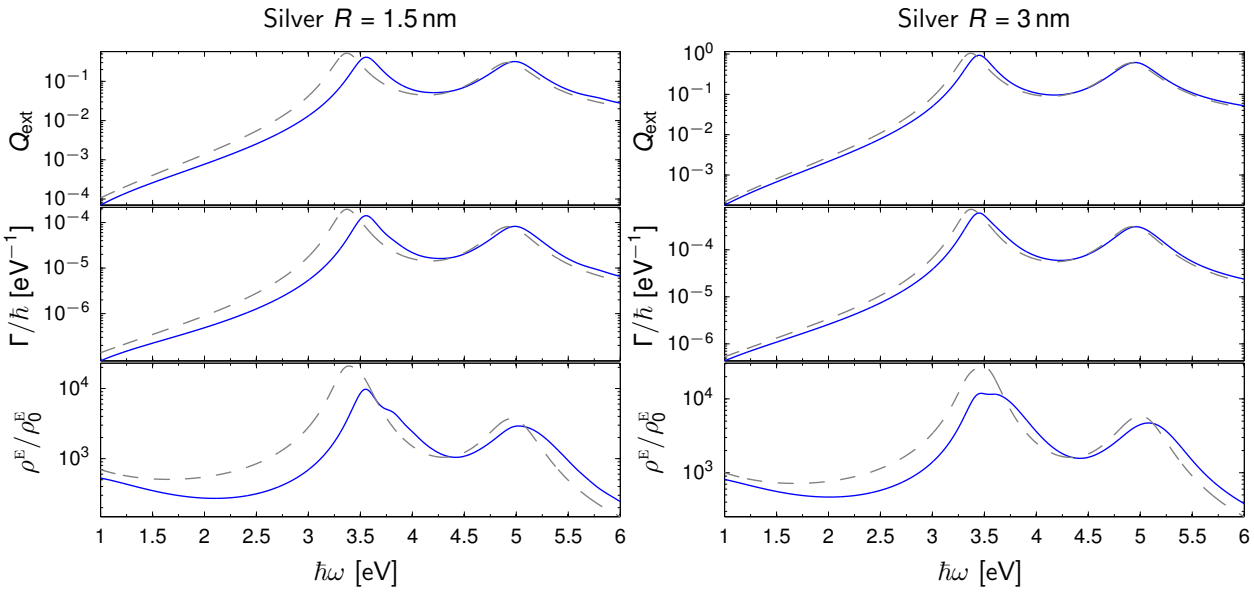

Figure S3: Extinction efficiency, EELS probability, and normalized LDOS. Setup parameters are identical to those in Figure S2, but for silver of two different radius. Probe-to-surface separation is $b - R = 1.5\,\mathrm{nm}$ in both cases. Hydrodynamics and LRA in full blue and dashed gray, respectively, as before. Experimental data for silver taken from Ref. S3, with free-electron parameters $\omega_{\mathrm{p}} = 9.01\,\mathrm{eV}$ and $\eta = 48\,\mathrm{meV}$.

References

(S1) Kittel, C. *Introduction to Solid State Physics*; Jon Wiley & Sons, 2005.

(S2) Rakić, A. D. Algorithm for the Determination of Intrinsic Optical Constants of Metal Films: Application to Aluminum. *Appl. Opt.* **1995**, *34*, 4755–4767.

(S3) Rakić, A. D.; Djurišić, A. B.; Elazar, J. M.; Majewski, M. L. Optical Properties of Metallic Films for Vertical-Cavity Optoelectronic Devices. *Appl. Optics* **1998**, *37*, 5271.

(S4) Stratton, J. A. *Electromagnetic Theory*; McGraw-Hill Book Company: New York, 1941.

(S5) Bohren, C. F.; Huffman, D. R. *Absorption and Scattering of Light by Small Particles*; John Wiley & Sons: New York, 1983.

(S6) Jackson, J. D. *Classical Electrodynamics*, 3rd ed.; John Wiley & Sons: New York, 1999.

(S7) García de Abajo, F. J. Optical Excitations in Electron Microscopy. *Rev. Mod. Phys.* **2010**, *82*, 209–275.

(S8) García de Abajo, F. J. Relativistic Energy Loss and Induced Photon Emission in the Interaction of a Dielectric Sphere with an External Electron Beam. *Phys. Rev. B* **1999**, *59*, 3095–3107.

(S9) Abramowitz, M.; Stegun, I. A. *Handbook of Mathematical Functions with Formulas, Graphs, and Mathematical Tables*; Dover: New York, 1972.

(S10) Kerker, M.; Wang, D.-S.; Chew, H. Surface Enhanced Raman Scattering (SERS) by Molecules Adsorbed at Spherical Particles: Errata. *Appl. Opt.* **1980**, *19*, 4159–4174.

(S11) Ruppin, R. Decay of an Excited Molecule near a Small Sphere. *J. Chem. Phys.* **1982**, *76*, 1681–1684.

(S12) Chew, H. Transition Rates of Atoms Near Spherical Surfaces. *J. Chem. Phys.* **1987**, *87*, 1355–1360.

(S13) Dung, H. T.; Knöll, L.; Welsch, D.-G. Decay of an Excited Atom near an Absorbing Microsphere. *Phys. Rev. A* **2001**, *64*, 013804.

(S14) Vos, W. L.; Koenderink, A. F.; Nikolaev, I. S. Orientation-Dependent Spontaneous Emission Rates of a Two-Level Quantum Emitter in any Nanophotonic Environment. *Phys. Rev. A* **2009**, *80*, 053802.

(S15) Datsyuk, V. V. Ultimate Enhancement of the Local Density of Electromagnetic States Outside an Absorping Sphere. *Phys. Rev. A* **2007**, *75*, 043820.

(S16) Olver, F.; Lozier, D.; Boisvert, R.; Clark, C. *NIST Handbook of Mathematical Functions*; National Institute of Standards and Technology, 2010.

(S17) Gradshteyn, I.; Ryzhik, I. *Table of Integrals, Series, and Products*, 7th ed.; Elsevier Academic Press, 2007.

(S18) David, C.; García de Abajo, F. J. Spatial Nonlocality in the Optical Response of Metal Nanoparticles. *J. Phys. Chem. C* **2012**, *115*, 19470–19475.

(S19) Fuchs, R.; Claro, F. Multipolar Response of Small Metallic Spheres: Nonlocal Theory. *Phys. Rev. B* **1987**, *35*, 3722–3726.

(S20) Raza, S.; Yan, W.; Stenger, N.; Wubs, M.; Mortensen, N. A. Blueshift of the Surface Plasmon Resonance in Silver Nanoparticles: Substrate Effects. *Opt. Express* **2013**, *21*, 27344–27355.

(S21) Barberán, N.; Bausells, J. Plasmon Excitation in Metallic Spheres. *Phys. Rev. B* **1985**, *31*, 6354–6359.

(S22) Vielma, J.; Leung, P. Nonlocal Optical Effects on the Fluorescence and Decay Rates for Admolecules at a Metallic Nanoparticle. *J. Chem. Phys.* **2007**, *126*, 194704.